Available online at www.academicpaper.org

Academic @ Paper

ISSN 2146-9067

International Journal of Automotive Engineering and Technologies
Vol. 3, Issue 1, pp. 1 – 21, 2014

International Journal of Automotive Engineering and Technologies

http://www.academicpaper.org/index.php/IJAET

Original Research Article

A Comparison of Flow Control Devices for Variable Geometry Turbocharger Application

Apostolos Pesiridis[1*], Botev Vassil[2], Muhammad Padzillah[2], Ricardo Martinez-Botas[2]

[1] Brunel University, United Kingdom
[2] Imperial College London, United Kingdom

Received 15 July 2013; Accepted 26 December 2013

Abstract

In this paper the aerodynamic performance of two common variable geometry inlet flow control devices for use in turbocharger turbines is investigated, namely: the pivoting vane and sliding wall flow restrictors, as well as a combination of the two mechanisms at the inlet to the turbine rotor, acting as coupled Active Control Turbocharger (ACT)/ Variable Geometry Turbine (VGT) mechanisms in series (one mechanism providing instantaneous area flow control for ACT – an instantaneous exhaust energy recovery capability; the other providing optimum mean nozzle position in conventional VGT mode), using computational fluid dynamics (CFD) techniques. The latter coupled study was carried out with the purpose to explore a more optimal application of turbine inlet flow control to an advanced ACT system. Numerical models of the stator passages for the different mechanisms were developed and a study of the flow unsteadiness based on the Strouhal number was performed. The latter found that the flow was quasi-steady allowing transient conditions to be modelled by superposition of steady state scenarios. The numerical models were subsequently validated using experimental data. An investigation of the NACA profile thickness of the pivoting vanes was also undertaken, the findings of which indicated that a NACA thickness of 0018 constituted the optimum compromise between increased velocity and incurred losses. The results for the pivoting vane simulations demonstrated the effect of loss mechanisms such as leakage and flow separation. It was established that the 65° vane angle delivered the highest velocity to the rotor, corroborating the earlier research findings. In the case of the coupled mechanisms, the main loss generating flow structure was found to be the large wake produced by the sliding wall, which significantly increased the inefficiencies through the stator. In comparison, the pivoting vane mechanism exhibited substantially lower levels of pressure losses and delivered higher velocities to the rotor.

Keywords: turbocharger, variable geometry, active control, pulsating flow

Nomenclature

ACT	Active Control Turbocharger	γ	Specific heat ratio	r	Radius
VGT	Variable Geometry Turbine	ζ	Loss coefficient	T	Temperature
FGT	Fixed Geometry Turbine	η	Efficiency	U	Blade Velocity
PS	Pressure Side	ρ	Density	St	Strouhal number
PV	Pivoting Vane	ω	Angular velocity	$\dot{W}$	Power
SS	Suction Side	A	Area	***subscript Θ***	Tangential property
SST	Shear Stress Transport	C	Flow velocity	***subscript n***	Nozzle
SW	Sliding Wall	h	Enthalpy	***subscript 0***	Stagnation property
LE	Leading Edge	$\dot{m}$	Mass flow rate	***subscript r***	Radial property
TE	Trailing Edge	M	Mach number	***subscript s***	Isentropic property
α	Absolute flow angle	p	Pressure	***subscript t-s***	Total to static
β	Relative flow angle				

* Corresponding author:
e-mail: apostolos.pesiridis@brunel.ac.uk

1. Introduction

Turbocharging is well established technology to increase power density in internal combustion engines. The demand for ever more advanced turbocharging concepts has increased in recent years as it has proven to be one of the major enabling technologies for engine downsizing. Engine downsizing – the reduction in engine swept volume with corresponding increase in power density to match earlier version of the same engine in naturally aspirated form – has come about as a technology roadmap of choice for engine manufacturers as a result of their need to accommodate ever stricter emissions legislations and the rising cost of petrol. As a result, turbocharger technologies have, over the past few decades, undergone significant developments such as the commercial introduction of variable geometry turbines (VGTs) which by incorporating a set of stator nozzles or other flow control devices can vary the inlet area of the turbine rotor thereby making better use of the entire exhaust energy content throughout the range of speed and loading conditions experienced during engine operation Pesiridis, 2007 [1]. Although VGTs do, to a certain extent, improve the energy harnessing capability of turbochargers, they are incapable of exploiting the highly pulsating nature of the exhaust gases fed into the turbine. To address this shortcoming, a further technology is currently under development, namely the Active Flow Control Turbocharger (ACT) which incorporates a mechanism enabling it to actively adapt the effective stator inlet area to the instantaneous exhaust pulse pressure.

The function of the turbine stator and actively controlled flow restrictors incorporated in the ACTs is to accelerate the flow of gas and channel the fluid into the rotor at the preferred angle with minimum incurred energy losses. In light of the above, it was crucial to study the aerodynamic performance of the flow restriction mechanism and determine the extent of the losses. This paper presents the performance of the various proposed ACT mechanisms through the use of both steady state and transient CFD simulations. It is based on the experimental results of testing of the two types of flow restrictor mechanisms studied: the sliding wall and pivoting vane flow restrictors (Figure 1). These two types of flow restricting mechanisms are by far the most widely employed types of flow control devices in VGTs today. In so doing, the paper endeavours to quantify the performance parameters and losses experienced during operation and identify the flow characteristics which lead to the inefficiencies, thereby leading to both a comparison of these two types for VGT application, as well as to lead to apply a novel scheme of matching the two systems in series for ACT operation and deliver a comparison of performance of the coupled systems. A study of the NACA thickness of the pivoting vanes is, also, presented, in order to investigate the effect of this consideration on the performance and efficiency of the ACT.

2. Background

The ACT mechanism was developed based on a modified version of the hardware found in VGTs. Two of the most commonly used flow restriction mechanisms found in commercially available VGT designs were adapted to function as the actively controlled components on ACTs. These are the pivoting vanes, shown in Figure 1 (a), and sliding nozzle ring, shown in Figure 1 (b).

The pivoting vane mechanism is comprised of a set of vanes distributed circumferentially along the stator inlet to the turbine rotor and are controlled by an actuating ring which, in ACTs, is driven by a high force, high response actuator. The pivoting vanes act like nozzles and as the vane angle is increased the effective inlet area to the turbine is reduced in the radial direction. In the case of the sliding wall-type nozzle ring mechanism, flow restriction is in the axial direction and is achieved by restricting the turbine inlet area using an

axially sliding wall. As first proposed by Pesiridis, 2007 [1], the ACT design adapts the rotor inlet area to the highly fluctuating pressure distribution observed in the exhaust gas flow. The concept is illustrated in Figure 2.

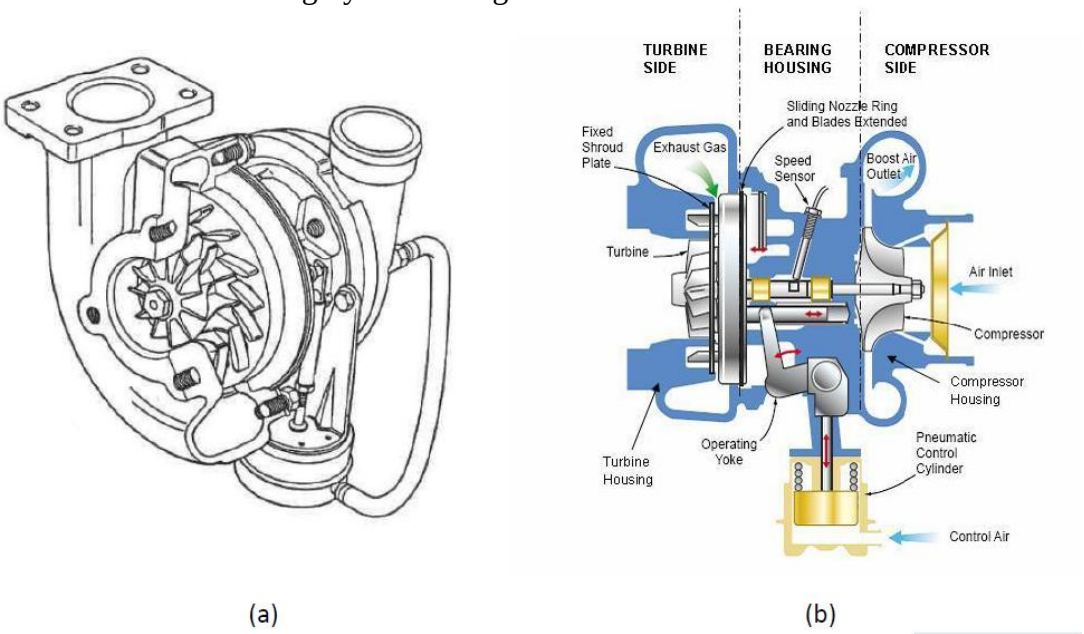

Figure 1 - (a) Pivoting vane VGT (Hiereth and Prenninger, 2003 [2]) and (b) sliding nozzle ring VGT (Cummins, 2001 [3])

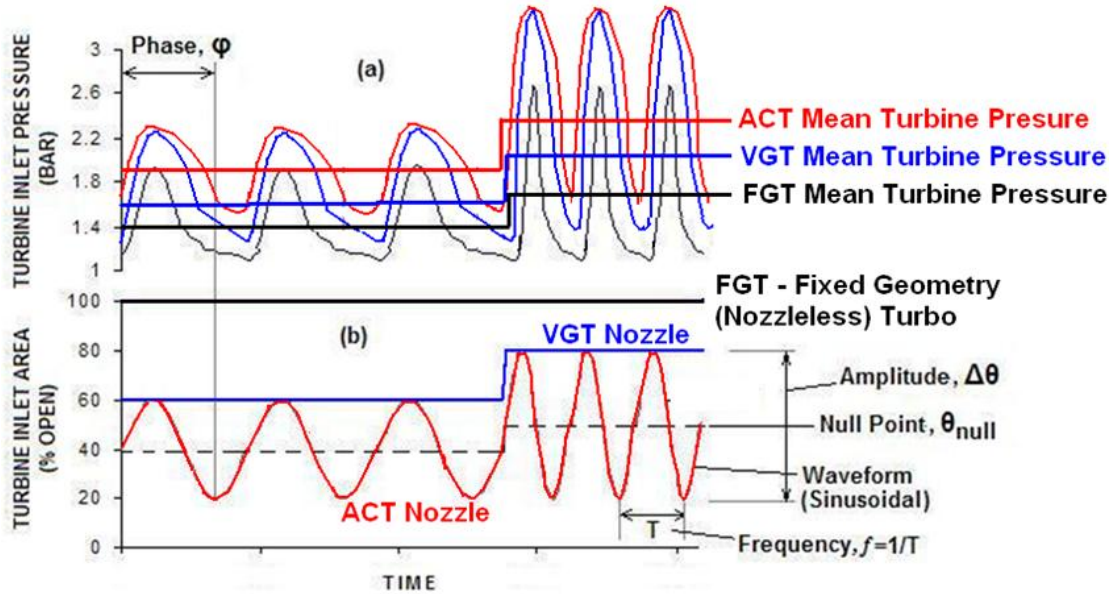

Figure 2 - Typical turbine inlet pressure profile (a) and the corresponding operating profiles of FGT, VGT and ACT turbine inlet area regulation schedules (Pesiridis, 2007) (b)

Pesiridis, 2007 [1] modified the sliding nozzle ring and actuated it using an electromagnetic shaker. This enabled both ACT and VGT capabilities as the amplitude of the oscillation could be varied depending on the speed and loading conditions while the frequency of oscillation was matched to the pulsating pressure profile of the exhaust gases. Although the design increased power output by between 3-7%, it was inherently prone to losses, Pesiridis and Martinez-Botas, 2007 [4].

A second ACT design was suggested by Rajoo, 2007 [5] who achieved flow restriction by using a ring of 15 pivoting vanes which rapidly oscillate between 40° (open position) and 70° (closed position) vane angles, also actuated by an

electromagnetic shaker. Similar to Pesiridis', 2007 [1] sliding wall mechanism, the pivoting vanes had coupled VGT and ACT capabilities. Overall, the pivoting vane ACT design was shown to be more efficient at extracting exhaust gas energy although it does have the disadvantage of being more complicated mechanically due to the large number of moving parts.

Due to the difficulty in employing a fast response actuator to cope with exhaust gas pulse frequencies of up to 60Hz in the laboratory environment or up to more than 100Hz on a real medium/heavy duty diesel engine, decoupling the ACT and VGT functions through the use of independent actuators, lends itself as an idea. For this to be practically feasible, the decoupling of the ACT and VGT functions was necessary with two separate flow restrictors acting in series. In order for the final area restriction to be the product of the individual contributions rather than the minimum of both, restrictors operating under different principles had to be used. In order to assess the performance of the various ACT designs a revision of radial in-flow gas turbine theory is called for and this is presented in the following paragraphs.

The schematic in Figure 3 shows a radial flow turbine with nozzle vanes distributed along the edge of the rotor inlet. The station numbering used in Figure 3 will be adopted to refer to performance parameters at the various locations. Nozzle vanes are used to accelerate the flow, whereby the pressure is reduced resulting in an increase of flow kinetic energy. The flow acceleration in the stator nozzles takes place between stations *1* to *2*. If this process is isentropic, the end point would be 2_S. As there is no work transfer through the stator, the stagnation enthalpy remains constant (neglecting heat transfer), so h_{01} is equal to h_{02}. However, stagnation pressure falls across the nozzle depending on the magnitude of the friction loss and incidence induced flow mechanisms. The nozzle efficiency, η_n, is therefore given by *Equation 1*, with an analogous definition given as a ratio of static and stagnation flow velocities, *C*, Dixon and Hall, 2010 [6].

$$\eta_n = \frac{h_{01}-h_2}{h_{01}-h_{2_S}} = \left(\tfrac{1}{2}C_2^2\right)/\left(\tfrac{1}{2}C_{2_S}^2\right) \qquad (1)$$

A common means of quantifying the energy losses in the stator nozzle is to express them as a dimensionless coefficient. The stagnation pressure loss coefficient, ζ, which will be used for the purposes of this report, is based on the ratio of the stagnation pressure drop across the nozzle to the dynamic head at stator exit, given by *Equation 2* (Simpson et al., 2009 [7]).

$$\zeta = \frac{P_{01}-P_{02}}{\frac{1}{2}\rho C_2^2} \qquad (2)$$

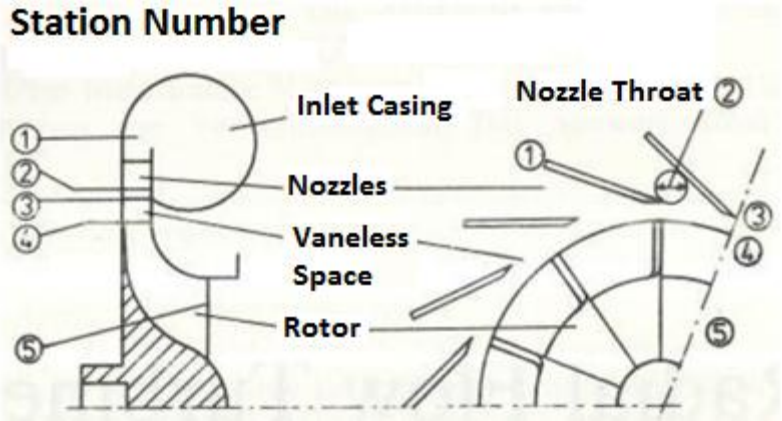

Figure 3 - Components of a radial flow turbine (Watson and Janota, 1982 [8])

Fundamentally, the turbine is designed to extract energy or work from the flow. Therefore, by comparing turbine power for different nozzle configurations, it is possible to ascertain which is performing best. Based on the velocity triangles for the turbine stage shown in Figure 4 the power can be defined as the rate of change of angular momentum

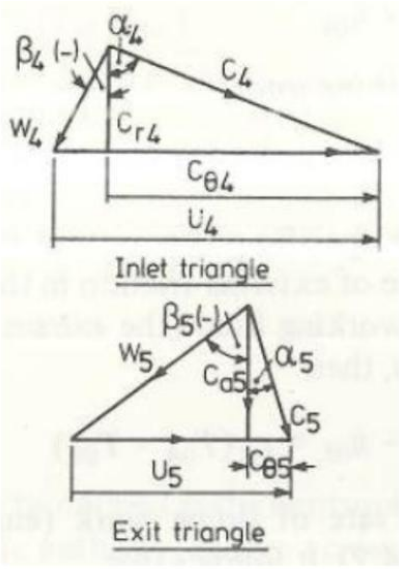

Figure 4 - Velocity triangles for radial turbine (Watson and Janota, 1982 [8])

of the flow. In practice, since it is desirable to minimize the kinetic energy at the exit of the turbine stage, it is usually arranged that the tangential component of absolute exit velocity, $C_{\theta 5}$, is zero, yielding the expression in *Equation 3.*

$$\dot{W} = \omega T = \dot{m}(U_4 C_{\theta 4} - U_5 C_{\theta 5}) \cong \dot{m} U_4 C_{\theta 4} \qquad (1)$$

As the development of the ACT was based on that of the VGT, literature on the latter is highly relevant to the study of the aerodynamics of flow restrictor devices. Spence et al., 2006 [9] studied the tip leakage flow loss mechanism which arises from the necessity to include a vane endwall clearance in the mechanical design of the turbine. The phenomenon was studied for the pivoting vane mechanism using a numerical model of a single passage of the stator and rotor with minimum and maximum vane angles. The results demonstrated that for the minimum vane angle, designed for higher flow rates, the flow structures were dominated by the effect of the turbulent wake induced by the high incidence angle. Leakage flow was also observed flowing in two directions, primarily from the pressure to the suction side. In the case of the maximum vane angle, the dominant structure was the leakage endwall clearance which was observed to flow in a single direction dictated by the blade loading. The numerical model was validated by comparing the blade loading results to experimental pressure readings along the surface of the stator vanes.

Table 1 - Description of the numerical methods employed in the study of the turbine stator

Author	Year	Analysis Type	Code	Domain	Number of Elements/Nodes	Turbulence Model	Boundary Conditions
Putra et al.	2006	Steady State	Fluent	Volute & vane passage	$2.2*10^6$ (nodes)	RSM and *k-ε*	N/A
Spence et al.	2006	Steady State	ANSYS CFX	Stator & rotor passage	Stator: 265 000 Rotor: 180 000 (elements)	SST	Inlet: Mass flow rate Outlet: Static pressure
Tamaki et al.	2008	Steady State	IHI developed code	Stator & rotor passage	Stator: 325 000 Rotor: 574 000 (nodes)	Spalart-Allmaras	Inlet: T_o, P_o Outlet: Static Pressure
Simpson et al.	2009	Steady State & Transient	ANSYS CFX	Full Stage	Stator passage: $1*10^6$ Rotor passage: $1*10^6$ (nodes)	SST	Inlet: T_o, P_o Outlet: Static Pressure

The effect of clearance flow was also investigated Tamaki et al. 2008 [10] who employed a similar numerical approach to Spence et al., 2006 [9]. It was noted that due to the leakage vortex, non-uniformity of the total pressure and flow angle in the entire

pitch direction near the wall is generated which causes mixing losses downstream of the vane. Simpson et al., 2009 [7] chose to model the full turbine stage in addition to the single stator/rotor passage in order to resolve the azimuthal non-uniformity of the flow around the volute. From the detailed single passage simulation Simpson et al., 2009 [7] noted the presence of horseshoe vortices emanating from the leading edge of the vane and propagating across the passage which drained a significant amount of low momentum boundary layer fluid into the centre of the passage. This low momentum flow and the wake coming off the trailing edge have a significant influence on the overall loss levels.

Table 1, indicates the corresponding characteristics from some of the simulation work in VGT flow restrictor devices.

3. Computational Methodology

The numerical modelling was carried out using the ANSYS V12.1 Computational Fluid Dynamics software package. Models were created for the pivoting vane ACT proposed by Rajoo, 2007 [5] and for both possible permutations of the coupled ACT/VGT mechanism described in the previous section. For the more complicated geometries of the coupled ACT/VGT mechanisms, it was necessary to also employ the Design Modeler and Mesh tools in addition to the turbomachinery tools such as Turbogrid and CFX.

The coupled pivoting vane ACT proposed by Rajoo, 2007 [5] was based on a mixed flow turbine with an arrangement of 15 nozzle vanes following the NACA 0015 airfoil profile distributed circumferentially along the stator shown in Figure 5. The outline of the mixed flow turbine is provided at the bottom of the figure, while the rectangular grey area in the diagram on the right of Figure 5 indicated the location within the turbine inlet passage of the straight vane (i.e., which is parallel to the axial disposition of the turbocharger turbine shaft and and does not feature any inclination angle to follow the angle of the leading edge of the mixed flow turbine.

The nozzle vanes are designed to pivot between 40° (open position) and 70° (closed position) angles measured from the radial direction. In order to study the transient ACT operation of the pivoting nozzle vanes, a VGT setting was chosen corresponding to a vane angle of 50°. As such, at this particular setting, the nozzle vanes oscillate between vanes angles of 50° to 70° following the operating schedule of the ACT relative to the pressure pulse. In this range, the investigated vane angles and corresponding inlet and outlet areas are given in

Table 1, where the outlet area relates to the nozzle throat as described in Figure 3.

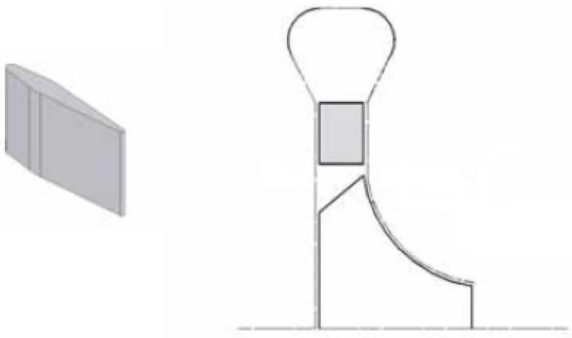

Figure 5 - Straight nozzle vane shape and meridional projection of the turbine Rajoo, 2007 [5]

Table 1 - Investigated vane angles and the corresponding inlet and outlet areas Rajoo, 2007 [5]

Model Number	Vane Angle [°]	Inlet Area (A1) [mm²]	Outlet Area (A2) [mm²]	Area Ratio (A2/A1)
1	50	325.33	147.99	0.455
2	55	322.49	122.97	0.381
3	60	319.83	101.76	0.318
4	65	317.36	78.68	0.248
5	70	315.1	55.63	0.177

As already mentioned the coupled mechanism was composed of both a pivoting vane ring flow restrictor assembly and a sliding wall flow restrictor each acting independently in fulfilling either the VGT or ACT function. Two possible designs were considered one with the sliding wall restrictor performing as ACT with the pivoting vanes, located upstream, performing the VGT function (appropriate mean area dependent on engine load and speed condition), and a second with the pivoting vane restrictor performing as ACT with the sliding wall, located upstream, to operate at the frequency of the incoming exhaust pulse as per Figure 2. The design employs a sliding wall with a thickness of 1mm, located on the hub wall of the turbine sliding axially outward toward the shroud and a volute and pivoting nozzle ring taken directly from Rajoo, 2007 [5].

With the two flow restrictors acting in series, the total area restriction (area ratio) is the product of the individual contributions of each mechanism. To ensure comparability between the flow restriction of the coupled ACT/VGT mechanism and the pivoting vane simulations shown in Table 1, the area ratios were sought to be matched. For the coupled mechanism with sliding wall acting as ACT and pivoting vane as a VGT, the key dimensions and settings are given in Table 3. For the sake of simplicity, a short-hand notation has been adopted with 'PV' and 'SW' referring to pivoting vane and sliding wall, respectively.

Table 2 - Dimensions and area ratios for the coupled mechanism with sliding wall as ACT and pivoting vane as VGT

Model Number	Corresponding Coupled Model Number	ACT: SW Distance [mm]	ACT: SW Area Ratio	VGT: PV Angle [°]	VGT: PV Area Ratio	Total Area Ratio
6	1	0	1.00	50	0.455	0.455
7	2	2.23	0.838	50	0.455	0.381
8	3	4.14	0.699	50	0.455	0.318
9	4	6.27	0.545	50	0.455	0.248
10	5	8.44	0.388	50	0.455	0.177

Table 3 - Dimensions and area ratios for the coupled mechanism with pivoting vane as ACT and sliding wall as VGT

Model Number	Corresponding Coupled Model Number	ACT: PV Angle [°]	ACT: PV Area Ratio	VGT: SW Distance [mm]	VGT: SW Area Ratio	Total Area Ratio
11	1	40.0	0.579	2.96	0.786	0.455
12	2	47.4	0.485	2.96	0.786	0.381
13	3	53.4	0.405	2.96	0.786	0.318
14	4	60.0	0.316	2.96	0.786	0.248
15	5	66.7	0.225	2.96	0.786	0.177
15*	5	54.6	0.388	7.52	0.455	0.177

For the coupled mechanism with the pivoting vanes functioning as ACT and the sliding wall as VGT, the key dimensions and settings are given in Table 4.**Hata! Başvuru kaynağı bulunamadı.**Ideally, for comparability, the area ratios of the ACT and VGT mechanisms would be equal to those of the configuration described in Table 3.

However, because the mechanical design of

the pivoting vanes assumes a minimum angle of 40°, it was not possible to match the area restriction contributions although their product, the total area ratio, was the same. At the maximum area restriction operating point (model number 15), this issue could be overcome, so model number 15* was included to allow for comparison of the mechanisms with identical settings. The created geometries can be seen in Figure 6.

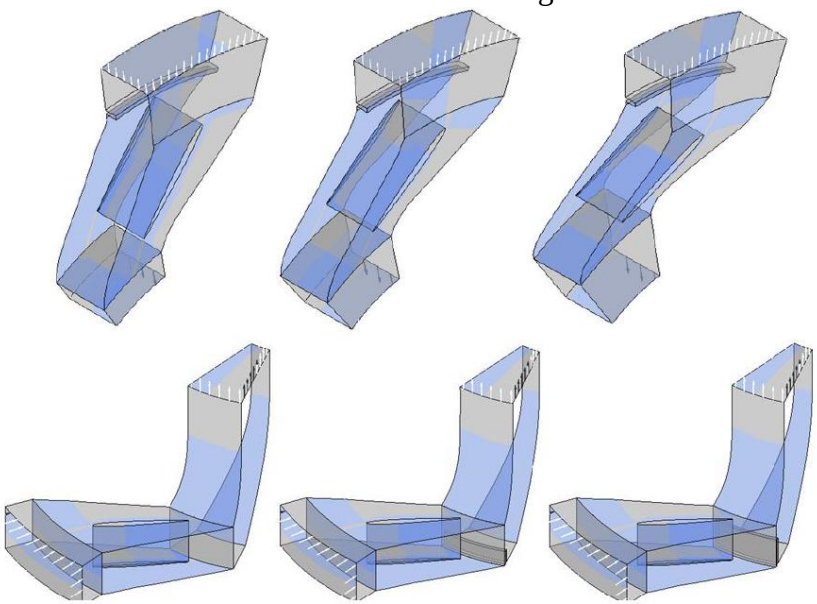

Figure 6 - Coupled mechanism geometries for Model Numbers 6, 8, 10 (from Table 3); all in top row (left to right), where ACT:PV and VGT:SW and in bottom row (from left to right) Model Numbers 11, 13, 15 (Table 4) where ACT:SW and VGT:PV

Once the pivoting vane geometries were created, they were imported into Turbogrid for the numerical grid generation. A hub endwall clearance of 0.215mm was introduced and an H/J/C/L grid type in conjunction with an O-Grid of width factor 0.2 was used as it was found to yield the best results in terms of mesh skewness. The number of elements was set to 280,000, and the tip clearance was modelled with 10 equispaced node points, which are similar values to those employed by Spence et al., 2006 [9]. Furthermore, as the SST turbulence model was employed, a y^+ value close to unity was required in order to resolve the details in the boundary layer.

The geometries for the sliding wall mechanism were imported into ANSYS Mesh for the generation of the numerical grid. A high quality mesh could be created by exploiting the axisymmetric geometry and using a sweeping method in conjunction with an inflated region near the fluid/surface interface to accurately resolve the flow in the boundary layer. This yielded a mesh size in the order of 70,000 elements for the passage with sliding wall functioning as VGT and 180,000 elements for the sliding wall functioning as ACT.

To simulate the inherently transient conditions during ACT operation without resorting to the use of computationally expensive dynamic meshes, an approach was adopted which relied on the superposition of steady state scenarios. The viability of this approach was demonstrated by evaluating the Strouhal number of the flow. The Strouhal Number (*St*) is a dimensionless parameter used in fluid mechanics to quantify the level of unsteadiness in a periodic flow Rajoo, 2007 [5]. In a turbocharger, the Strouhal number is used to evaluate the significance of the unsteady dynamics in the volume (pipes and stator) compared to the pulsating event of the flow. Equation 8 is the expression for the Strouhal Number in its generic form, where ω is the frequency of the disturbance, L is a characteristic length, and U is the velocity of the fluid, White, 2010 [12].

$$St = \frac{\omega L}{U} = \frac{Convective\ Timescales}{Disturbance\ Timescales} \qquad (4)$$

The Strouhal number can be evaluated for the stator by taking the characteristic length, *L*, to be the chord of the nozzle vane and the fluid velocity, *U*, to be the passage averaged velocity from the leading edge to the trailing edge of the blade. When the Strouhal number is low ($St < 0.1$), the flow may be considered quasi-steady and the transient analysis can be performed by superposition of steady state scenarios (Rajoo, 2007). After evaluating *St* for the investigated simulations it was found that this condition is satisfied, demonstrating the validity of the approach used for this project.

The original conception of the ACT is presented in Figure 7, whereby a sinusoidal area regulation was superimposed on the pressure profile of one exhaust pulse. From the figure, it may be appreciated that the constant VGT area coincides with the peak of the sinewave in ACT operation at the time instant when peak pressure occurs, Pesiridis, 2007 [1]. As explained earlier, for the scenarios which are to be investigated in this project, a VGT setting equivalent to a 50° pivoting vane angle was selected. A sinusoidal ACT area regulation was then superimposed with the crest of the sinewave coinciding with the VGT area at peak pressure (50° vane angle) and the trough with maximum area restriction (70° vane angle).

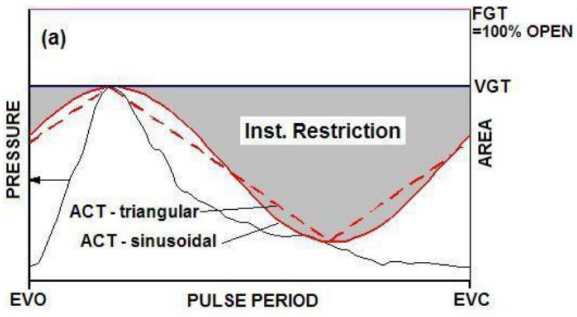

Figure 7 - Superposition of ACT sinusoidal turbine inlet area regulation schedule on a typical pressure profile during one exhaust cycle (Pesiridis, 2007)

Having established the area regulation schedule, the boundary conditions for the numerical models could be defined based on experimental measurements at the entry to the volute and then defined on CFX-Pre. A number of different configurations were investigated but the most robust was found to be a combination of specifying total pressure and temperature at inlet and mass flow rate at outlet of the computational domain. The static pressure at the outlet and velocity at inlet are thus part of the solution. This combination is also recommended in the ANSYS user guide for being amongst the most robust. Table 5 presents the boundary conditions which were used for the numerical models. The boundary conditions, given in Table 4, specified total pressure and temperature at inlet and mass flow at outlet of the domain. At the inlet, the flow direction was set to match the volute delivery flow angle of 68°, measured from the radial direction, by applying the assumption of free vortex flow to the scroll (Rajoo, 2007). For model numbers 6 to 10 the solution domain outlet had to be extended with a section of bladeless rotor (seen in Figure 6) as the significant wake which was being created by the sliding wall was reversed over the span of the boundary, thus detrimentally affecting the accuracy of the results (Tu et al. 2008 [11]). Similarly to Spence et al., 2006 [9] and Simpson et al., 2009 [7], the Shear Stress Transport (SST) turbulence model was adopted. For model numbers 6-10, the *k-ε* model had to be used as the extended solution domain made convergence more computationally demanding and could not be achieved with the criterion of 10^{-5} for the RMS of the residuals used throughout.

The design of the pivoting nozzle vanes is affected by a number of considerations which include: number of vanes, solidity, profile thickness and camber. Rajoo (2007) employed vanes with a NACA 0015 profile thickness but his choice was not extensively verified by experimental of theoretical evidence as to whether it constitutes an optimum for the given application. Therefore the current investigation will endeavour to study the influence of the NACA thickness on the performance of the nozzle vanes. It will do so by assuming steady state conditions and by implementing exhaust profile averaged boundary

conditions. To ensure the study is parametric, identical boundary conditions and nozzle vane angles were used for all the investigated NACA thicknesses. The inlet boundary conditions were set to a total pressure and temperature of 243.2kPA and 1173°K respectively, and a mass flow outlet boundary condition of 0.023kg/s per passage was specified. A vane angle of 65° was used throughout as this was the value cited by Rajoo (2007) for peak turbine efficiency. The investigated NACA profiles are given in Figure 8 where the relevant numbers indicate percentage thickness with respect to chord length i.e., 0021 refers to a thickness of the aerofoil section of 21% compared to the chord length.

Table 4 - Boundary conditions for the numerical modelling of the stator passage

Model Numbers	Total Pressure (Inlet) [kPa]	Total Temperature (Inlet) [°K]	Mass Flow Rate per Passage (Outlet) [kg/s]	Specific Heat at Constant Pressure (c_p) [J/kgK]
1,6,11	306.63	1299.3	0.021	1245.4
2,7,12	225.42	1109.8	0.031	1214.5
3,8,13	200.73	1036.5	0.032	1185.5
4,9,14	183.82	991.6	0.0295	1171.7
5,10,15,15*	198.11	985.7	0.0214	1171.7

Figure 8 - Investigated NACA profiles and their related thickness designation

Validation of the numerical models was performed by comparing experimental pressure readings along the vane pressure and suction surfaces (see Figure 9, where the exhaust flow would be entering from right to left in the figure) to computational blade loading data from the simulations. Rajoo, 2007 [5] conducted experimental testing of the vaned turbine stator in a cold flow test rig by observing the similarity approach of the performance parameters to ensure equivalence with actual conditions. The equivalent flow properties were determined to equate to a mass flow rate per nozzle vane passage of 0.01kg/s and a total pressure and temperature of 153.6kPa and 863°K respectively. The specified flow properties were used to define the boundary conditions of the pivoting vane numerical model for the 40° and 60° vane angles as these were tested by Rajoo, 2007 [5]. In order to evaluate the modelling error involved in the simulations both the SST and *k-ε* turbulence models were tested since they were both employed in the numerical models. The adopted numerical validation approach is similar to that used by Spence et al., 2006 [9] and Tamaki et al., 2008 [10].

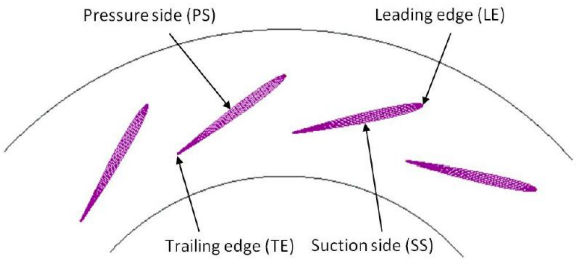

Figure 9 - Terminology used in describing the nozzle vane geometry

4. Computational Validation

The validation procedure for this work was performed for steady flow conditions and followed work by Padzillah et al., 2012 [13]. This validation procedure was employed to

demonstrate the capability of the CFD solver to capture with adequate prediction accuracy for subsequent scrutiny of the numerical results. For validation purposes, a full stage numerical model of a VGT was compared with the experimental data of Rajoo, 2007 [5]. The selected vane angle was 60^0 with the rotor rotating at 50% design speed which is equivalent to 30,000 rpm. The inlet condition was set to match the cold flow experimental condition. On the other hand, at the domain outlet, the ambient pressure and temperature were specified. The validation process did not include the sliding wall due the absence of equivalent experimental results. Nevertheless, the validation using the computational model of VGT in absence of sliding wall was sufficient to ensure the viability of the CFD prediction results.

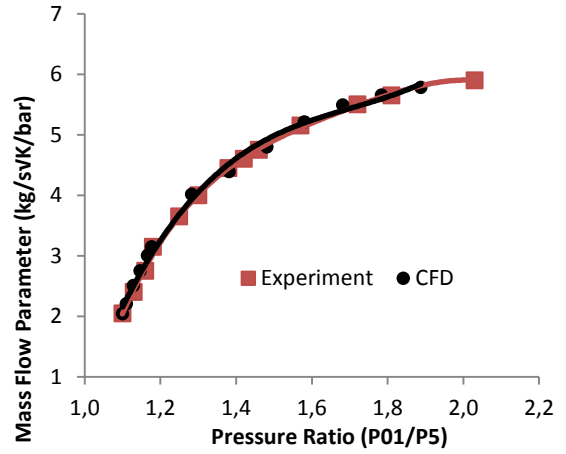

Figure 10 - Comparison between CFD and experimental results for (a) Mass Flow Parameter and (b) Total-to-static Efficiency

Figures 10(a) and (b) show the comparison between CFD and experimental data for the turbine mass flow parameter and its efficiency. Figure 10(a) indicates that the mass flow as the domain exit boundary condition is predicted accurately by the CFD model throughout the operating pressure ratio. However, the efficiency plot indicated in Figure 10(b) recorded a slight under prediction of 1% at the peak efficiency point. In general, one would expect that the CFD model would over predict the efficiency throughout the operating velocity ratio due to the absence of mechanical loss and backdisk friction loss prediction capability which could only be uncovered in experimental test results. Despite this loss of resolution within a narrow map range, the data obtained from the numerical model is still well within the experimental uncertainty limit, which is calculated to be up to 7% at highest velocity ratios [5]. The comparison of the CFD model with experimental results has yielded satisfactory agreement and therefore it is concluded that the subsequent work to investigate the flow behaviour in the vane domain could represent the actual condition.

In addition to the validation process using a full stage VGT performance map, the static pressure on the vane surfaces was also used as one of the validation parameters. The comparison was made between the single passage CFD model of the vane and experimental results. Figure 11 and Figure 12 show comparisons of experimental (Rajoo SS and PS referring to Rajoo, 2007 [5] aerofoil's suction ad pressure surfaces, respectively) and numerical static pressure (P_S) data for the 40° and 60°vane angles, respectively, which have been normalised by the total pressure at inlet to the volute (P_{01}).

As may be observed from Figure 12, the pressure and suction side lines cross over after the blade leading edge for both the measured and predicted data, indicating that the flow experiences incidence.

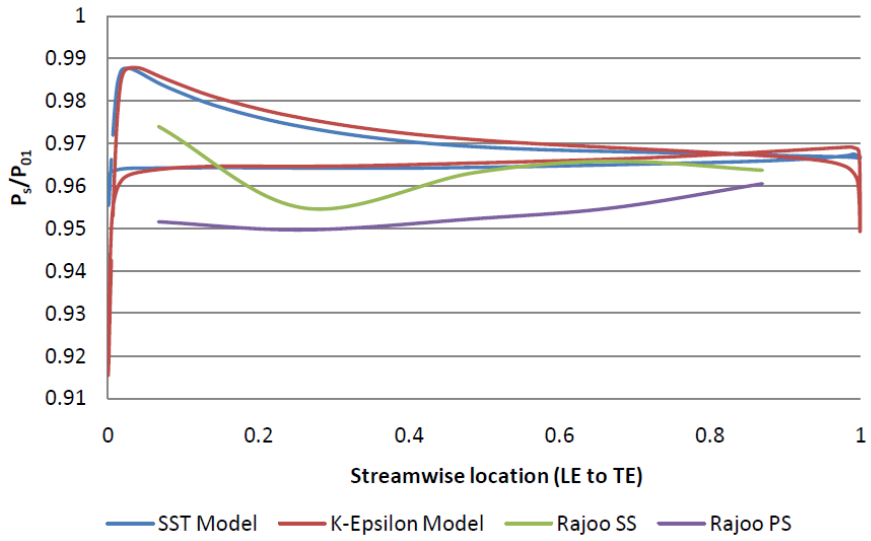

Figure 11 - Numerical blade loading predictions for the 40° vane angle plotted alongside normalised static pressure measurements on vane surface at 50% span

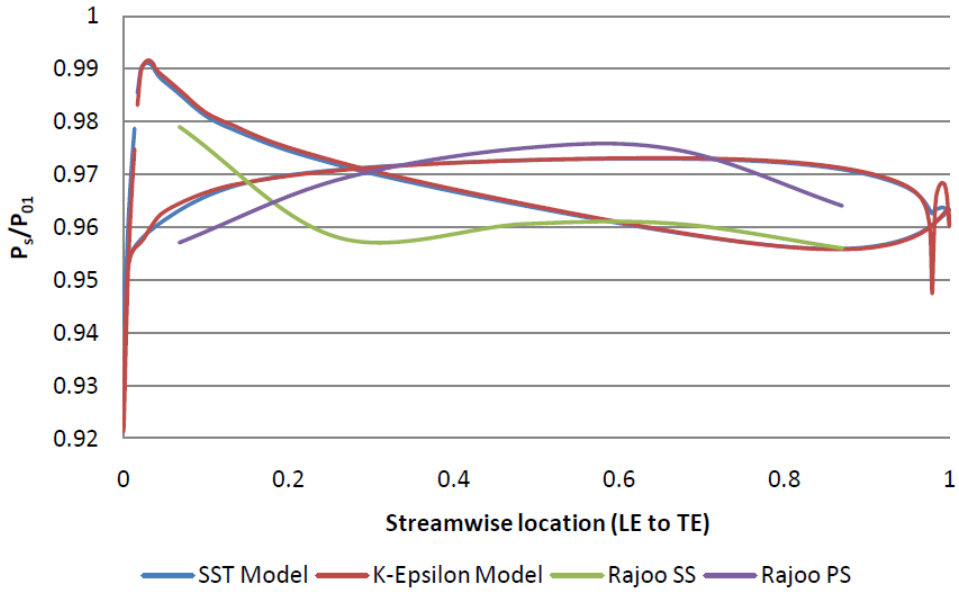

Figure 12 - Numerical blade loading predictions for the 60° vane angle plotted alongside normalised static pressure measurements on vane surface at 50% span

The predicted pressure variation suggests that a greater degree of negative loading is encountered than was observed from the measured results, which implies that the theoretical flow angle of 68° delivered by the scroll may deviate somewhat from the actual conditions where the flow is less tangential. The vertical misalignment which is apparent in the plots of both the 40° and 60° vane angles could be attributed to the assumption used when specifying the inlet boundary conditions that total conditions are equal to those at entry to the volute. This is of course is a simplification as pressure losses will occur in the volute casing.

The two tested turbulence models show excellent agreement in both the 40° and 60° vane angle plots. This may not come as a surprise as the SST was partially based on the k-ε model, but it does suggest that the coupled models with ACT: SW and VGT: PV which had to be simulated using the k-ε, for the reasons detailed in the previous section, are not significantly compromised in terms of accuracy. The close agreement in the predictions of the two turbulence models does breakdown somewhat at the trailing

edge of the vane. The capacity of the k-ε model to resolve the turbulent wake is not as refined when compared to the SST model, explaining the predicted behaviour at the trailing edge. Generally, however, there is good agreement between the numerical predictions and experimental data which suggests that the modelling errors are acceptable.

5. Results

The profile thickness of the nozzle vanes has several repercussions on the performance of the stator. Blades which are thin will have a smaller surface area and as a result will experience less skin friction losses making the nozzle more efficient. However, they will also have a larger throat area as compared to thicker blade which detrimentally affects the flow acceleration through the nozzle, and will generally not be as successful at guiding the flow at the desired angle, leading to higher deviation which is the difference between the flow and nozzle chord angles.

The results of the investigation are given in Figure 13 and Figure 14. As may be observed, the higher the NACA profile thickness, the larger the Mach number, deviation and pressure loss coefficient, defined by *Equation 2*. Given that the primary function of the stator nozzles is to accelerate the flow entering the rotor in order to impart a greater momentum transfer, the Mach number is the parameter of greatest importance, followed by the nozzle efficiency, deviation and pressure loss coefficient. From the above prioritisation, the optimal trade-off between a high Mach number and low levels of nozzle inefficiency are achieved at a NACA profile thickness of approximately 0018. However, for the best performing nozzle profile thickness to be determined it is necessary to take into account considerations other than the aerodynamic performance such as the associated mass of the vanes and the consequences this has on actuation.

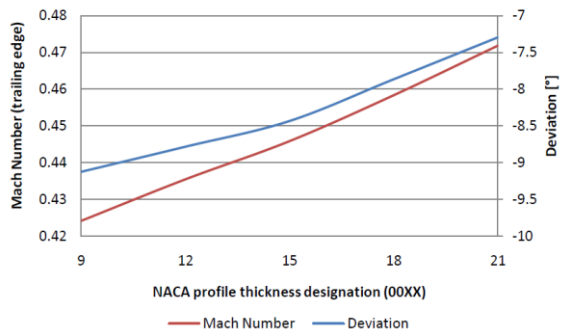

Figure 13 - Plot of pressure loss coefficients and nozzle efficiency for the investigated profile thicknesses

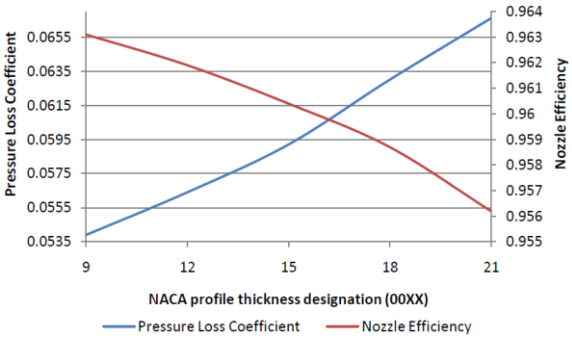

Figure 14 - Plot of Mach number and deviation for the investigated profile thicknesses

5.1 Coupled Mechanism: VGT: SW with ACT: PV

For the sake of efficiency in the reporting process, only worst case scenario flow mechanisms will be discussed and presented graphically which occur under maximum (Model Number 5) and minimum (Model Number 1) flow restriction operating conditions.

For model number 1, the velocity vector plots are shown in Figure 15. As may be seen for Figure 15(b), the flow for this condition experiences considerable incidence at the nozzle leading edge of 23.1°. This results in a region of flow separation along the pressure surface of the vane. Although the separated flow can be seen to reattach towards the trailing edge, the recirculation produces a significant amount of low momentum fluid which emerges downstream of the nozzle in the wake. This non-uniformity of the flow is likely to lead to further inefficiency through the rotor.

Another flow mechanism which contributes to the losses in the stator was the leakage flow, is illustrated in Figure 15(a). The

leakage can be observed to flow in two directions; first from suction to pressure side due to the incidence angle, and then from pressure to suction side as a result of the blade loading shown in Figure 17. This effect was similar to that observed by Spence et al., 2006 [9] who noted that the shearing action which results from the movement of the leakage flow relative to the mainstream passage flow forces a layer of fluid to roll in to the core of a vortex.

For model number 5, the velocity vector plots are shown in Figure 16. In this case the incidence angle was at a minimum of 4.0° (see Table 6) so no flow separation was observed. However, the blade loading shown in Figure 18, is significantly higher than for model number 1 and gives rise to leakage flow from the pressure to the suction side of the vane across its length illustrated in Figure 16(a). This effect was also noted by Tamaki et al., 2008 [10] for the minimum opening vane angle.

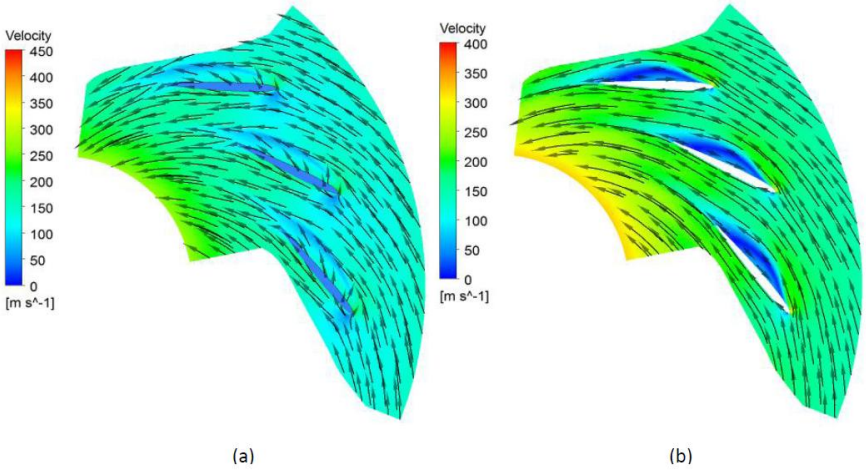

Figure 15 - Velocity vector plots for model number 1 in the clearance plane (a) and at mid-span blade-to-blade plane (b)

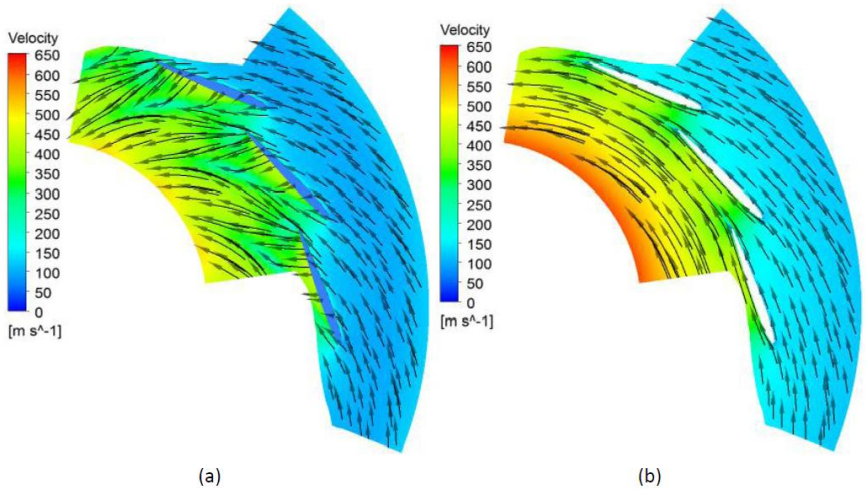

Figure 16 - Velocity vector plots for model number 5 in the clearance plane (a) and at mid-span blade-to-blade plane (b)

Table 5 - Pivoting vane nozzle performance parameters from LE to TE

Model Number	Nozzle Efficiency (η)	Pressure Loss Coefficient (ζ)	Incidence [°]	Deviation [°]
1	0.9214	0.1214	23.1	-6.42
2	0.9601	0.0624	18.1	-7.37
3	0.9648	0.0556	13.3	-7.89
4	0.9598	0.0671	8.48	-8.12
5	0.9374	0.0792	4.02	-10.1

Table 6 - Average flow conditions at entry to the rotor stage given at 50% span of the rotor leading edge

Model Number	Total Pressure [kPa]	Total Temperature [°K]	Mach Number	Tangential Velocity ($C_{\theta 4}$) [m/s]	Absolute Flow Angle (α_4) [°]	Relative Flow Angle (β_4) [°]
1	302.99	1299.27	0.390	234.36	60.70	-11.10
2	220.36	1109.77	0.640	357.29	62.86	27.84
3	193.70	1036.43	0.788	433.09	66.70	42.78
4	170.19	991.54	1.09	569.84	68.05	53.79
5	183.83	985.63	0.899	504.00	74.88	61.59

The performance parameters for the nozzle vanes are given in Table 6. Model number 3 (60° vane angle) has the highest nozzle efficiency but from the velocity data given in
Table 6 and *Equation 3*, it seems that the highest momentum transfer in the rotor will occur for model number 4 (65° vane angle), also cited by Rajoo, 2007 [5] as the maximum turbine efficiency condition.

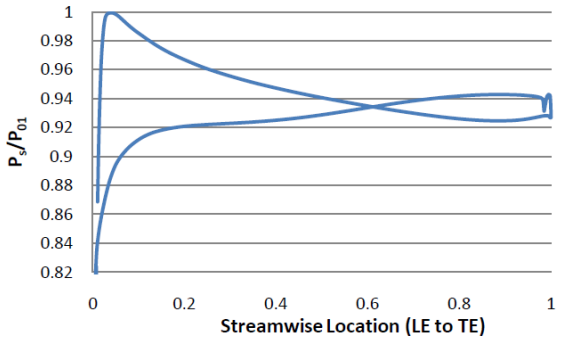

Figure 17 - Normalised blade loading for model number 1

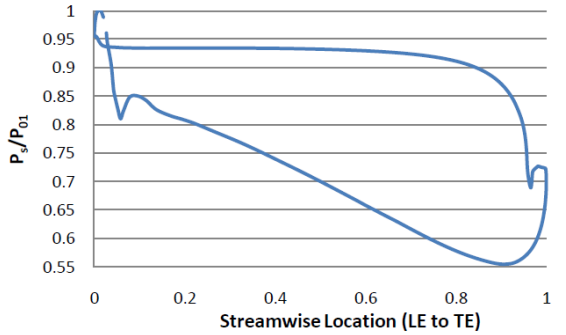

Figure 18 - Normalised blade loading for model number 5

A similar approach to that used in the previous section, will be adopted in the treatment of the coupled mechanisms, whereby only the two extreme conditions (model numbers 11 and 15) will be discussed. For model number 11, the velocity vector plots are given in Figure 19. As may be observed from Figure 19(b), which is given in the plane of the sliding wall perimeter, a substantial degree of flow disturbance and non-uniformity is produced by the wall which forms a large region of low momentum fluid. This turbulent wake region dramatically affects the flow conditions entering the downstream nozzle vanes and results in an incidence angle of 35.7° (see also Table 7), which severely impairs their performance. The effects of the incidence angle compounded with the large wake coming off the sliding wall generate a substantial region of low momentum flow on the pressure side of the vanes which causes blockage of the passage, resulting in a corridor of high velocity flow along the suction surface. Leakage, caused by the blade loading, is illustrated in Figure 19 flowing from suction to pressure side of the vane. The combined effect of the aforementioned flow mechanisms was a highly non-uniform flow entering the turbine rotor as is apparent from Figure 21(a) and (b). As a result of the important loss mechanisms, the coupled nozzle performs significantly worse than its decoupled counterpart (model number 1), indicated by the performance parameters in Table 7.

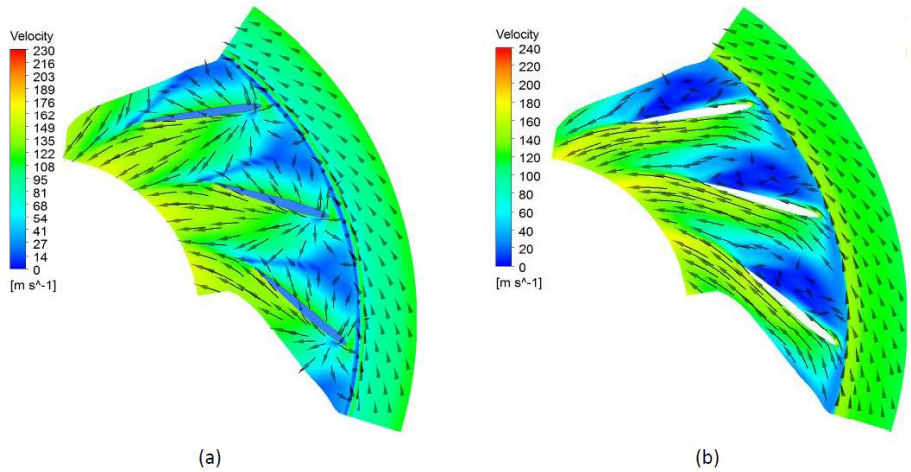

Figure 19: Velocity vector plots for model number 11 in the clearance plane (a) and at 20% span blade-to-blade plane (b)

Table 7: Decoupled mechanism nozzle performance parameters from leading face of SW to trailing edge of PV

Model Number	Nozzle Efficiency (η)	Pressure Loss Coefficient (ζ)	Incidence (for PV) [°]	Deviation (for PV) [°]
11	0.7778	0.3909	35.74	-4.897
12	0.8349	0.2573	27.34	-5.287
13	0.8934	0.1523	20.82	-5.893
14	0.9300	0.1003	13.94	-7.705
15	0.9349	0.0927	7.68	-8.835
15*	0.8350	0.2509	20.36	-5.367

Table 8 - Average flow conditions at entry to the rotor stage given at 50% span of the rotor leading edge

Model Number	Total Pressure [kPa]	Total Temperature [°K]	Mach Number	Tangential Velocity ($C_{\theta 4}$) [m/s]	Absolute Flow Angle (α_4) [°]	Relative Flow Angle (β_4) [°]
11	303.23	1299.3	0.2230	125.41	54.803	-57.02
12	218.36	1109.8	0.4672	253.27	58.760	-3.04
13	194.12	1036.5	0.6144	332.29	62.570	22.32
14	176.72	991.57	0.7764	419.09	66.842	41.78
15	190.85	985.67	0.6905	392.59	73.347	49.16
15*	192.39	985.67	0.4112	228.13	66.414	-17.93

For model number 15, the velocity vector plots are shown in Figure 20. In this case, the nozzle vanes are rotated to a more tangential position, resulting in a larger interspace between the leading edges and the sliding wall. As a result, the wake from the sliding wall has a greater vaneless space over which to diffuse and its effects on the nozzle vanes are considerably reduced when compared to model number 11. The incidence angle at the leading edge was 7.68° (see Table 7) which leads to an overall better performing ring of nozzle vanes. Although flow separation did not occur, the leakage loss mechanism is still exhibited by the flow, as shown in Figure 20. The vortex which is formed as a result of the leakage produces a noticeable disturbance in the flow immediately downstream of the vane trailing edge. In this scenario, the presence of the nozzle vanes downstream of the sliding wall was able to re-channel the wake coming off the wall and deliver a near uniform flow to the turbine rotor inlet which may be observed from Figure 21(c) and (d). However, the coupled nozzle still performs worse than the equivalent setting of the decoupled pivoting vane (model number 5) with a nozzle efficiency and pressure loss coefficient deterioration of -0.3% and 17% respectively (see Table 7). Furthermore, the ideal comparison of the ACT/VGT functions in the coupled and decoupled mechanisms, given by model number 15*, demonstrates that with the sliding wall extended further into the stator passage, the performance parameters of the nozzle are significantly worsened due to the larger wake and incidence. From the figures in Table 7, model number 15 seems to have the best nozzle performance. However, the flow conditions at entry to the turbine rotor given in Table 12 suggest that the overall turbine performance of the model number 14 will be superior since the higher tangential velocity ($C_{\theta 4}$) delivered to the rotor will impart a greater momentum transfer, as dictated by *Equation 3*. **Hata! Başvuru kaynağı bulunamadı.** suggests that the overall turbine performance of the model number 14 will be superior since the higher tangential velocity ($C_{\theta 4}$) delivered to the rotor will impart a greater momentum transfer, as dictated by *Equation* 3.

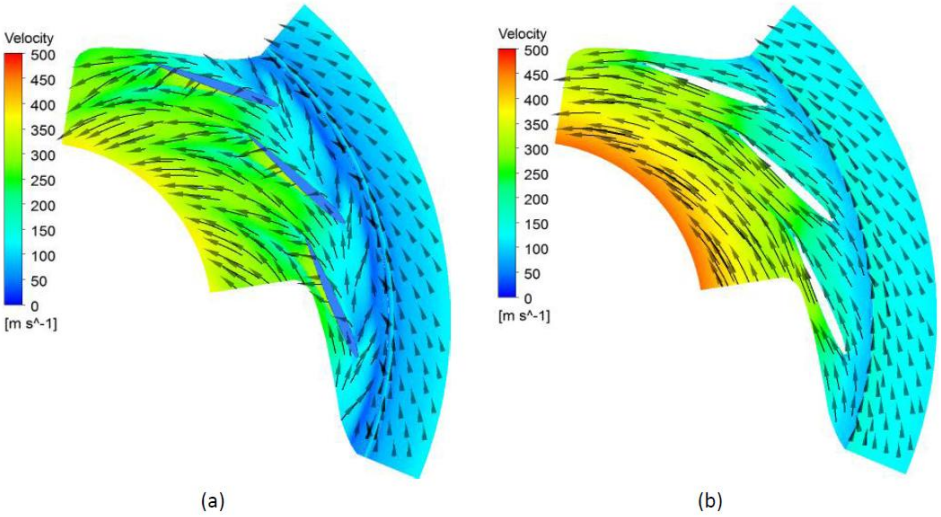

Figure 20: Velocity vector plots for model number 15 in the clearance plane (a) and at 20% span blade-to-blade plane (b)

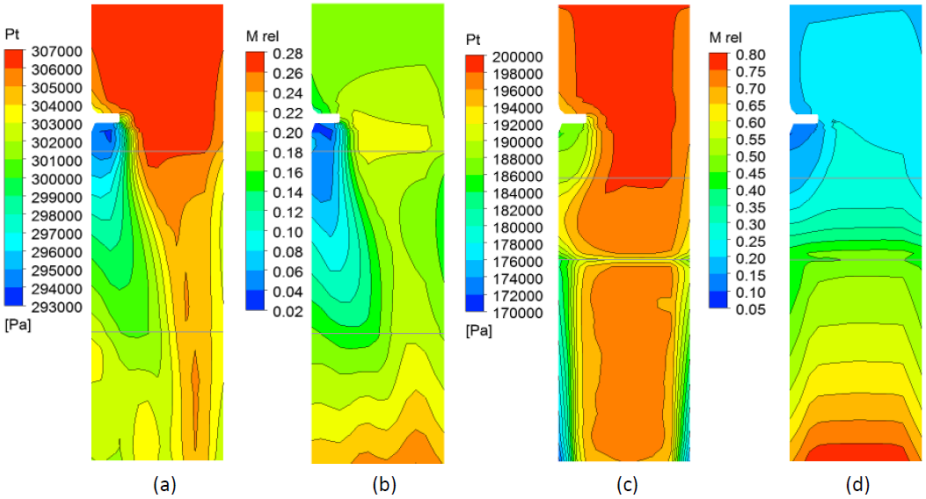

Figure 21 - Meridional contour plots of total pressure (a), (c) and Mach number (b), (d) for model number 11 and 15 respectively. The grey horizontal lines indicate the leading and trailing edges of the nozzle vanes.

5.2 Coupled Mechanism: VGT:PV with ACT:SW

As before, only the two worst case scenarios will be presented graphically. However, in this case model number 6 which constitutes the scenario with least flow restriction was effectively analogous to the condition presented for the 50° vane angle (model number 1) as the sliding wall was fully retracted. Model number 7 will therefore be discussed instead in addition to the maximum flow restriction scenario (model number 10).

For model number 7, an incidence angle of 22.7° encountered at the leading edge (see Table 9) causes the flow to separate along the pressure surface of the vane. Due to the presence of the sliding wall downstream, the flow field was distorted, as may be seen in Figure 22, with the higher pressure and velocity flow skewed toward the shroud. The incidence at the leading edge also creates leakage flow from the suction to pressure surface of the vane. The combined effect of the separation and leakage on the pressure losses can be seen by the low pressure regions in Figure 23 at the vane trailing edge. Further pressure losses are incurred from the wake generated by the sliding wall, creating highly unfavourable flow conditions at the rotor inlet. Consequently, the mixed flow rotor geometry is likely to prove highly inefficient as was noted for a similar configuration by Pesiridis, 2007 [1].

Table 9 - Decoupled mechanism nozzle performance parameters from leading edge of PV to trailing face of SW

Model Number	Nozzle Efficiency (η)	Pressure Loss Coefficient (ζ)	Incidence (for PV) [°]	Deviation (for PV) [°]
6	0.9158	0.1255	23.16	-6.30
7	0.9060	0.1496	22.75	-6.55
8	0.9254	0.1922	22.65	-6.56
9	0.9134	0.3736	22.71	-6.41
10	0.8907	0.7412	23.07	-5.66

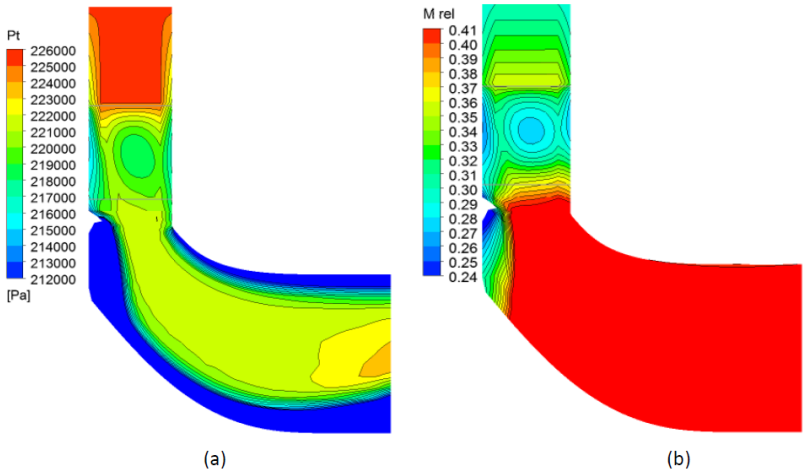

Figure 22 - Meridional contour plots of total pressure (a) and Mach number (b) for model number 7. The grey horizontal lines indicate the leading and trailing edges of the nozzle vanes.

Figure 23 - Circumferential contour plot of total pressure at vane trailing edge for model number 7

For model number 10, flow separation was again apparent as a result of the incidence at the blade leading edge. With the sliding wall extended further into the passage, the distortion of the upstream flow field through the nozzle vanes was even more severe (Figure 24), leading to growth of the separation at a spanwise position near the shroud endwall. The leakage flow pattern was similar to that discussed for model number 7 with the flow travelling from suction to pressure surface. The resultant pressure losses are apparent in Figure 25 for the flow delivered by the nozzle vanes. With the sliding wall extended to its maximum position, the created wake spans more than half of the stator passage and contributes to the highest pressure loss coefficient for the investigated nozzles of 0.74 as shown in Table 9. As a result, the pressure loss coefficients are on average 59% higher than those for the coupled mechanism with VGT: SW and ACT: PV and 310% higher than those for the decoupled pivoting vanes. However, the calculated nozzle efficiencies are surprisingly high for the witnessed

degree of inefficiency. This could be due to the position at which the nozzle efficiency was measured (from LE of PV to trailing face of SW) which was adapted from the theory for classical nozzle vanes in order to suit the sliding wall mechanism. It is possible that if the measurement location were moved to a further downstream position where the wake has mixed out, the calculated nozzle efficiencies would have been lower. A further explanation maybe found in the discrepancy in the numerical solution as a result of the inability of the employed *k-ε* turbulence model to resolve the boundary layer effects as well as the SST model.

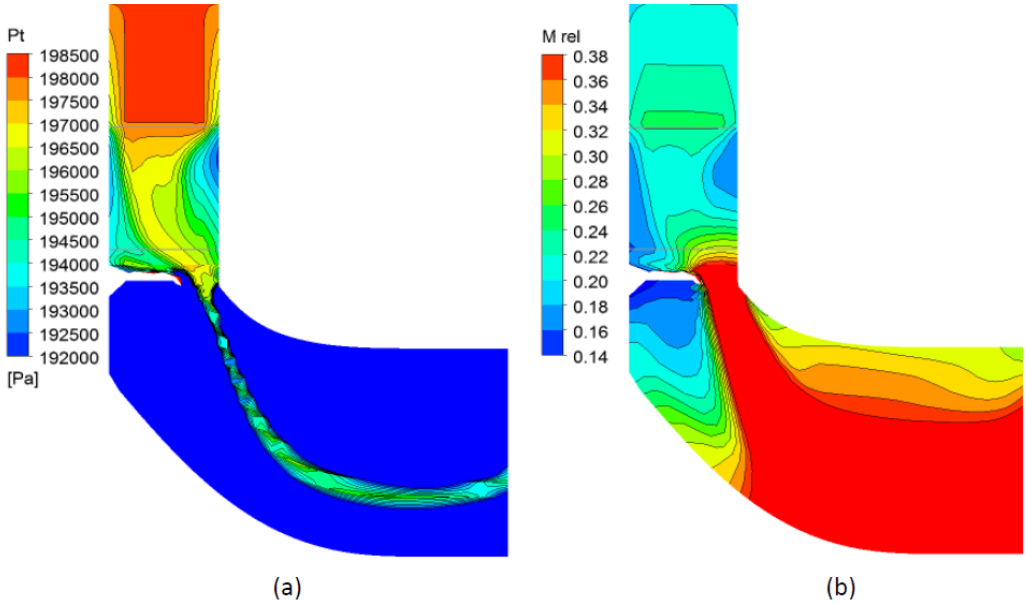

Figure 24 - Meridional contour plots of total pressure (a) and Mach number (b) for model number 10. The grey horizontal lines indicate the leading and trailing edges of the nozzle vanes.

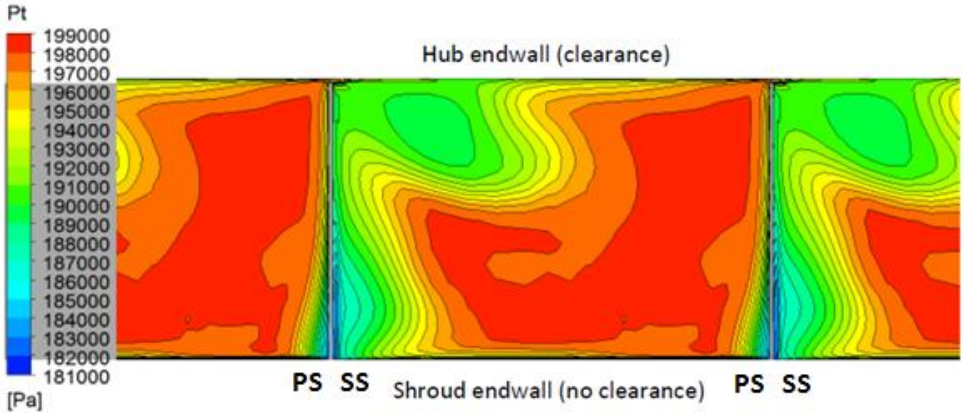

Figure 25 - Circumferential contour plot of total pressure at vane trailing edge for model number 10

Table 10: Average flow conditions at entry to the rotor stage given at 50% span of the rotor leading edge

Model Number	Total Pressure [kPa]	Total Temperature [°K]	Mach Number	Tangential Velocity ($C_{\theta 4}$) [m/s]	Absolute Flow Angle (α_4) [°]	Relative Flow Angle (β_4) [°]
6	304.47	1299.29	0.243	152.72	66.17	-57.86
7	219.26	1109.78	0.456	231.00	65.18	-14.02
8	192.54	1036.45	0.563	233.80	66.13	-11.69
9	173.77	991.45	0.647	191.60	67.61	-24.95
10	189.15	985.58	0.533	117.81	72.01	-51.33

The nozzle efficiency figures suggest that model number 8 has the best performance and this was corroborated by the high tangential velocity given in Table 10. Comparing the different ACT mechanisms which have been investigated in this project, the highest momentum transfer in the rotor, as per the given velocity data, will occur in the decoupled pivoting vane mechanism. In comparison, the coupled mechanism with VGT: SW and ACT: PV performs less well by 26.5%, followed by the coupled mechanism with VGT: PV and ACT: SW which incurs a performance drop of 59.0%. Although this seems to be compelling evidence in favour of the decoupled ACT mechanism, a complete assessment of the different options would require more than an aerodynamic evaluation and would involve further studies into the feasibility of decoupling the ACT/VGT functions and cost analysis in order to determine the financial benefits of implementation.

6. Conclusions

The present work presented a study into the two most common types of flow restricting devices at the inlet to a Variable Geometry Turbocharger (VGT) turbine: a sliding wall nozzle and a pivoting vane nozzle. A study of their aerodynamic characteristics was carried out followed by a study of the two systems coupled in series for the advanced application of the Active Control Turbocharger (ACT). The two devices covered operation of the main VGT mode as well as the ACT mode with each being swapped to cover both cases: a sliding wall acting as a VGT upstream of a pivoting vane restrictor acting as an ACT and vice versa.

Numerical models of the pivoting vane mechanism and the coupled ACT/VGT mechanisms were successfully created and validated (section 4). A study of the transient conditions was performed based on the Strouhal number which found that the transience could be modelled using superposition of steady state simulations as the flow was quasi-steady.

An investigation of the NACA profile thickness of the pivoting vane mechanism was also performed which proposed that a NACA thickness of 0018 would constitute an optimum compromise between flow acceleration and incurred losses. The results of the pivoting vane simulations demonstrated that at large vane angles the flow field is dominated by the effects of leakage whereas at small vane angles the predominant loss mechanism is flow separation caused by the large incidence at the leading edge. The 65° vane angle was found to deliver the highest velocity to the rotor, corroborating the findings of Rajoo 2007 [5] who cites this operating condition as yielding the highest turbine efficiency.

The main loss generating flow structure for the coupled mechanisms was the large wake produced by the sliding wall. In both of the investigated permutations of the mechanism, the presence of the sliding wall was found to significantly affect the performance of the pivoting vanes. Compared to the coupled ACT pivoting vane mechanism, the coupled mechanisms exhibited substantially higher levels of pressure losses and lower velocities at inlet to the turbine rotor. However, the coupled mechanism with VGT: SW and ACT: PV performed noticeably better than the alternative arrangement, primarily due to higher exit velocities but also because of flow uniformity into the rotor.

7. References

1 Pesiridis, A. Turbocharger Turbine Unsteady Aerodynamics with Active Control. PhD Thesis, Imperial College London, 2007.

2 Hiereth, H. and Prenninger, P. Charging the Internal Combustion Engine. Vienna, Springer-Verlag, 2003.

3 Cummins. HY-40V Service Manual, Part No. 4029521. 2001.

4 Pesiridis, A. and Martinez-Botas, R. Experimental Evaluation of Active Flow Control Mixed-Flow Turbine for Automotive Turbocharger Application,

Journal of Turbomachinery, January 2007, Volume 129, Issue 1, pp. 44-52.

5 Rajoo, S., Pesiridis, A. and Martinez-Botas, R.F., Novel Method to Improve Engine Exhaust Energy Extraction with Active Control Turbocharger (ACT), International Journal of Engine Research, doi:10.1177/1468087412472414, March 1, 2013

6 Dixon, S. L. and Hall, C. A. Fluid Mechanics and Thermodynamics of Turbomachinery. Sixth edition. Burlington, Elsevier, 2010.

7 Simpson, A.T. Spence, S.W.T. and Watterson, J.K. A Comparison of the Flow Structures and Losses Within Vaned and Vaneless Stators for Radial Turbines. ASME Journal of Turbomachinery, [Online] 131 (3), 2009.

8 Watson, N. and Janota, M. S. Turbocharging the Internal Combustion Engine. Macmillan, London, 1982.

9 Spence, S. W. T., O'Neill, J. W. O. and Cunningham, G. An investigation of the flowfield through a variable geometry turbine stator with vane endwall clearance. Proceedings of the Institution of Mechanical Engineers, Part A, Journal of Power and Energy, 220 (A8), 899-910, 2006.

10 Tamaki, H., Goto, S., Unno, M. and Iwakami, A. The Effect Of Clearance Flow Of Variable Area Nozzles On Radial Turbine Performance. Proceedings of ASME Turbo Expo, 2008.

11 Tu, J. Yeoh, G. H. and Liu, C. (2008) Computational Fluid Dynamics: A Practical Approach. Amsterdam, London: Butterworth-Heinemann, 2008.

12 White, Frank M. (2010) Fluid Mechanics. seventh edition edition. New York, McGraw-Hill Higher Education.

13 Padzillah, M.H., Rajoo, S., and Martinez-Botas, R.F. (2012) Numerical Assessment of Unsteady Flow Effects on a Nozzled Turbocharger Turbine, Proceedings of the ASME Turbo Expo, 2012.